International Journal of Automation and Computing 17(2), April 2020, 279-291
DOI: 10.1007/s11633-018-1155-6

Modeling of a Smart Nano Force Sensor Using Finite Elements and Neural Networks

Farid Menacer Abdelmalek Kadr Zohir Dibi

Advanced Electronics Laboratory, Department of Electronics, University of Batna,
Avenue Chahid Boukhlouf Mohamed El Hadi, Batna 05000, Algeria

Abstract: The aim of this work is to model and analyze the behavior of a new smart nano force sensor. To do so, the carbon nanotube has been used as a suspended gate of a metal-oxide-semiconductor field-effect transistor (MOSFET). The variation of the applied force on the carbon nanotube (CNT) generates a variation of the capacity of the transistor oxide-gate and therefore the variation of the threshold voltage, which allows the MOSFET to become a capacitive nano force sensor. The sensitivity of the nano force sensor can reach 0.124 31 V/nN. This sensitivity is greater than results in the literature. We have found through this study that the response of the sensor depends strongly on the geometric and physical parameters of the CNT. From the results obtained in this study, it can be seen that the increase in the applied force increases the value of the MOSFET threshold voltage V_{Th}. In this paper, we first used artificial neural networks to faithfully reproduce the response of the nano force sensor model. This neural model is called direct model. Then, secondly, we designed an inverse model called an intelligent sensor which allows linearization of the response of our developed force sensor.

Keywords: Nano force, sensor, carbon nanotube (CNT), finite elements, neural network.

1 Introduction

In recent years, micro and nano force measurement has become a major problem for many applications, particularly in areas such as micro-assembly and micromanipulation. A force sensor is a device combining electronics and mechanics, it converts an applied force into an electrical signal.

All the micro or nano force sensors are based either on the measurement of the displacements of a non-deformable solid or on the measurement of the deformations of an elastic microstructure. Therefore, the unknown force must be deduced from the knowledge of these displacements or deformations by means of appropriate sensors.

The importance of force measurement on a micro or nano-scale has led to numerous prototypes of micro and nano force sensors. Most of these prototypes have sensitive elements (SE) that are passive elastic microstructures. These sensors differ by the means used to measure the deformation of the SE. For example, the atomic force microscope (AFMs) with 4-segment photodiode[1] or interferometer[2], the piezoresistive force sensors[3] that use the variation of resistance when an external force is applied to them, the piezoelectric force sensors[4] generating a potential difference in the presence of an external force field, the capacitive force sensors[5] based on the principle of change of capacitance induced by the change of distance between two metal plates after the application of an external force. Among the many sensors and sensing devices studied and developed, micro beam-based sensors show a large number of published works on the subject. The micro-beams have wide ranges of sensitivities, which are particularly interesting for applications in the fields of safety, the environment, industrial process control, product quality and health.

The literature on micro beam force sensors indicates numerous publications on the subject. For example, silicon micro-beams are used for the calibration of mechanical pen meter type instruments[6]. Silicon micro-beams are also used to control the applied forces by micromanipulators[7].

Some researchers developed a nano-scaled force sensor based on a photonic crystal which can be used to measure the component force in X and Y directions[8, 9].

The advancement of the nano and micro-electromechanical systems (NEMS/MEMS) technology to obtain nano force sensors of increasing sensitivity leads to the use of sensors of sub-micrometric or nanometric size. The carbon nanotubes, by their size and aspect ratio, coupled to their mechanical rigidity are very good nano-sensors.

In this paper, we propose a nano sensor specifically designed to detect and measure the force at the nanonewton scale, using a structure consisting of a suspended carbon nanotube with both of its ends embedded.

The nano force sensor can be operated in a static operating mode. In the static mode, the force applied to the

Research Article
Manuscript received December 3, 2017; accepted August 23, 2018; published online December 6, 2018
Recommended by Associate Editor Xun Chen

nano force sensor disrupts the balance of forces (moments) acting in the transducer and consequently induces a mechanical movement of the movable element which allows the transducer to reach a new state of mechanical equilibrium.

The difference between this state and the initial one is then used to measure this applied force. The detection of the deflection can also be deduced by a capacitive measurement. For this, we used the carbon nanotube as the suspended gate of a metal-oxide-semiconductor field-effect transistor (MOSFET). The distance between the gate and the transistor oxide has a capacity, the deflection of the nanotube then induces a variation of this capacitance. The use of the clamped-clamped (C-C) structure in the static mode for the detection of nano force is a particularly effective concept in terms of sensitivity and relatively simple to implement because it requires no actuating device.

We are also interested in this article to design a neural model of the nano force sensor based artificial neural networks (ANNs) approach. This model is implemented as a component in the library of the Oregon computer-aided design (ORCAD)-personal computer simulation program with integrated circuit emphasis (PSPICE) electrical simulator. This component must accurately express the behavior of the sensor. A second model based on neural networks, which will deal with the correction and compensation of the sensor output signal, has been designed and implemented on the same simulator, while eliminating the non-linearity of the sensor. Taking into account the complexity of the relation between inputs and outputs, the results obtained are very encouraging and satisfactory and lead us to understand that a good prediction requires the use of an optimal number of neurons in the hidden layer and a sufficient amount of data.

2 Structure of single wall carbon nanotube (SWCNT)

Since the discovery in 1991 by Sumio Iijima of the surprising electrical[10], mechanical and thermal properties of carbon nanotubes, the scientific and industrial world has studied the different fields of their application. A carbon nanotube results from the winding of one or more sheets of graphene on themselves. In the case where there is only one graphene sheet, a single wall carbon nanotube (SWCNT) is obtained. In the contrary case, where several sheets of graphene have been wound on themselves and have thus given a tube consisting of several tubes concentrically nested each into the other, we obtain what is called a multi wall carbon nanotube (MWCNT)[11]. In addition, there are various types of winding that can be described with the chirality vector. A graphene plane has a "honeycomb" type structure, i.e., it is formed by a periodic succession of carbon hexagons (benzene) of a_1 and a_2 basis vectors. The chirality vector is then defined as the winding vector of the nanotube. This chirality vector is decomposed according to the two vectors a_1 and a_2 forming the graphene base (Fig. 1). Thus, by introducing a couple of integers (m, n), the chirality vector is defined according to the relation 1[12]:

$$C_h = m \times a_1 + n \times a_2. \tag{1}$$

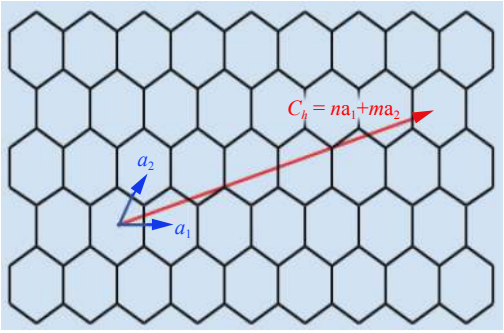

Fig. 1 Two dimensional hexagonal network of graphene[12]

Depending on the couple (m, n), three types of carbon nanotubes result, Armchair nanotubes are defined by $n=m$, Chiral nanotubes are defined by $n\neq m\neq 0$ and zigzag nanotubes are defined by $n=0$. These different types of nanotubes have mechanical, thermal and, above all, electrical properties specific to themselves[13]. The mechanical properties of carbon nanotubes are also used to realize the nano electro mechanical systems (NEMS). These include, the random access memory (RAM)[14], the rotating cylinders, the nano levers with feedback[15], the photomechanical actuators, the transparent resistive electrodes, the flexible light emitting diodes (LEDs), and more. All the geometrical characteristics of the nanotubes derive from the knowledge of the couple (n, m).

The nanotube diameter is given by the expression $D = \dfrac{d_{cc}\sqrt{3\,(n^2+m^2+nm)}}{\pi}$, d_{cc} is the carbon-carbon bond length (about $1.44\,A°$) and the chiral angle is defined according to the relation 2 with $|\theta| \in [0, 30°]$[16].

$$\theta = \arcsin\left|\frac{\sqrt{3m}}{2\sqrt{n^{2+m^2}+nm}}\right|. \tag{2}$$

2.1 Modeling of carbon nanotube by finite elements

The finite element method is widely used today to simulate the physical behavior of structures and systems (mechanical, thermodynamic, acoustic, etc.). In numerical analysis, the finite element method is used to numerically solve partial differential equations. Concretely, this method makes it possible to analyze complex structures by decomposing them into elements more regular in form, which will be described and solved by linear partial differ-

ential equations. The accuracy of the simulation depends on the density of the mesh, but also on the choice of the elements, these elements are the basic cell for the calculation.

The finite element simulation software that we use is analysis of systems (ANSYS); it is one of the widely used tools in the finite element method (FEM) analysis area, which allows analysis on several physical behaviors in different modes: static, dynamic, modal, temporal, etc. First of all in this study, we have developed a three dimensional model of the carbon nanotube based on the finite elements in Fig. 2. The modeling was done using the ANSYS calculation software based on the theoretical basis described in [17]. In this modeling, we have retained a type of structural element that can define the elementary beam of the carbon nanotube model: this element is called beam 188. The mechanical and geometrical properties of this element are presented in Table 1 below. This simulation is based on an energy equivalency method to pass an energy model (quantum mechanics) to structural mechanics[18, 19].

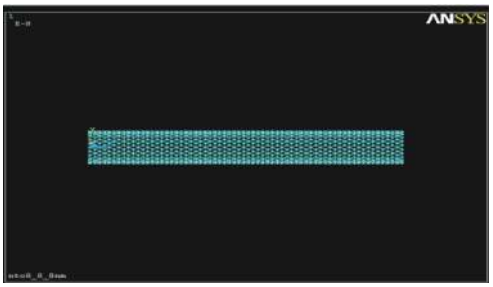

Fig. 2 Carbon nanotube model developed by the finite elements using ANSYS simulator

Table 1 Mechanical and geometrical properties of beam elements[18, 19]

Parameters	Value
Diameter of the nanotube d	1.466 $A°$
Length of carbon-carbon bond L	1.421 $A°$
Area of cross-sectional A	1.68794 A^2
Polar inertia momentum I_{xx}	0.453456 A^4
Inertia momentum I_{zz}=I_{yy}=I	0.22682 A^4

The beam 188 element corresponds to the beam elements, working in traction, compression, bending and flections and torsion. This element has three degrees of freedom at each node: the translations along the x and y directions and the rotation around the nodal z axis.

To validate our developed FEM model, we have taken an example of a nano-resonator studied by Wu et al.[20] presented in Fig. 3. For this, we used the carbon nanotube model developed as a resonant sensor, in a clamped-free configuration for species detection. The detection method is based on the variation of the resonance

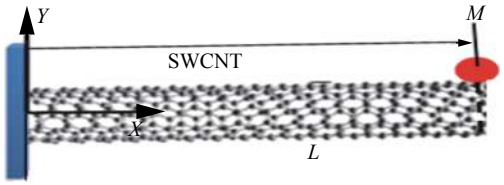

Fig. 3 A cantilever carbon nanotube biosensor developed by Wu et al.[20]

frequency of the resonator, whose change in the effective mass of the resonator induced by the mass added in end of the nano-resonator causes a change in its resonance frequency.

Our numerical simulation results are compared with the theoretical results and with the study carried out by Wu et al.[20]

It can be seen from Table 2 that our FEM simulation results are in good agreement compared with the theoretical and literature results.

Table 2 Resonant frequency for clamped-free resonator based SWCNT with different attached mass

Attached mass (Fg)	Theoretical values (Hz)	FEM simulated by [20]	Our FEM simulation
20	2017274.93	2025396.28	2019969.33
22	1938830.63	1945438.16	1954100.24
24	1868879.03	1874251.81	1881115.19
26	1805990.60	1810343.33	1835466.45
28	1749051.48	1752552.38	1754325.64
30	1697179.17	1699961.81	1700023.25

2.2 Study of the carbon nanotube deflection

We proposed to study the deflection of a carbon nanotube clamped at its two ends (bridge structure). This constitutes the sensitive element, which is presented in Fig. 4 (a), with length L, diameter D, the elasticity modulus is $E = 2.038$ Tpa, the Poisson′s coefficient is 0.30 and the mass density is 1330 kg/m^3 subjected to a concentrated force F[21]. When the carbon nanotube is subjected to a force, generally all the points of the carbon nanotube change position and the constraints are exerted on the three axes. The displacement of a point is defined as the distance between its initial position and its final position.

The general equations of the mechanics are presented by (3)–(5).

$$S_x = \frac{1}{E}T_x - \frac{\gamma}{E}T_y - \frac{\gamma}{E}T_z \tag{3}$$

$$S_y = -\frac{\gamma}{E}T_x + \frac{1}{E}T_y - \frac{\gamma}{E}T_z \tag{4}$$

$$S_z = -\frac{\gamma}{E}T_x - \frac{\gamma}{E}T_y + \frac{1}{E}T_z \tag{5}$$

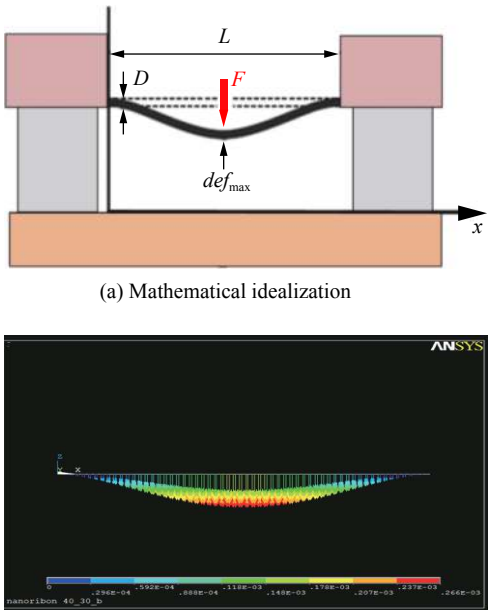

(a) Mathematical idealization

(b) ANSYS Simulation.

Fig. 4 Schemes of a nanotube subjected to a point force

where S_x, S_y and S_z represent the relative elongations along the three axes (x: parallel to the length, y: parallel to the width and z: parallel to the thickness). T_x, T_y and T_z represent the stresses along the three axes, E represents the Young's modulus and γ represents the Poisson's coefficient. In mechanics, generally when $D \ll L$, then we consider that $T_y = T_z = 0$ and the mechanical equations are summarized by (6):

$$S_x = \frac{1}{E}T_x,\ S_y = -\frac{\gamma}{E}T_x \ \text{ and } \ S_z = -\frac{\gamma}{E}T_x. \tag{6}$$

The formula describes the deflection def of the clamped-clamped nanotube (bridge structure), as a function of the applied force position, and is given by (7).

$$def = \frac{Fx}{48EI}\left(3L^2 - 4x^2\right) \ \text{ with } \ 0 \le x \le \frac{L}{2} \tag{7}$$

where I is the moment of inertia of the nanotube, x is the applied force position. When a force F is applied to the center of a clamped-clamped structure, this force will cause maximum deflection at this point, the maximum deflection is described by (8):

$$def_{\max} = \frac{FL^3}{48EI}. \tag{8}$$

The three-dimensional finite element ANSYS simulator is designed to calculate the deflection of the carbon nanotube FEM model (Fig. 4 (b)). Fig. 5 shows the maximum deflection variation at the center of the nanotube as a function of the applied force, we observe that the rate of deflection is a straight line. It can be concluded that the maximum deflection at the center of the nanotube is directly proportional to the applied force. The maximum deflection of a nanotube (9,9) with length 200 nm is 5.551 0 nm and 3.091 8 nm for an applied force 9 nN and 5 nN, respectively.

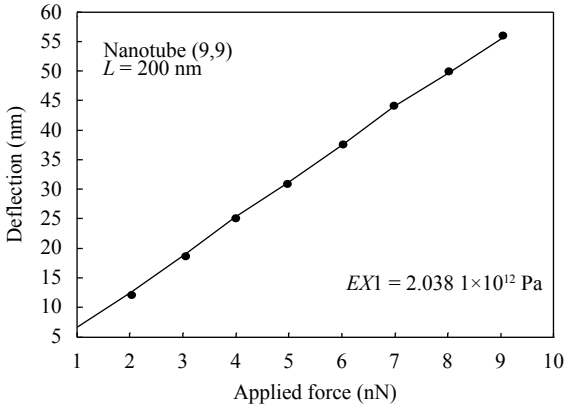

Fig. 5 Variation of the maximum deflection at the center of the nanotube as a function of the applied force

2.3 Influence of geometric parameters on deflection

In order to study the influence of the different geometric and physical parameters on the nanotube's deflection, we have simulated the deformation, and more particularly the maximum deflection, as a function of the length, the chirality and the nanotube's Young's modulus.

A first series of calculations corresponded to a fixed nanotube chirality of $n = 9$ and lengths varying between 130 nm and 200 nm. The results of the simulations are shown in Fig. 6.

The sensitivity to applied force is an essential characteristic for defining the performance of a force sensor. The sensitivity to the applied force is defined by (9).

$$S(F) = \frac{\Delta def}{\Delta F}. \tag{9}$$

A second series of calculations corresponds to a fixed length of 200 nm and chiralities varying between $n = 7$ and $n = 10$, the results of the simulations are shown in Fig 7.

According to Fig. 6 (a) and Fig. 7 (a), it is clear that for a fixed applied force, the more the length of carbon nanotube is high and its diameter is small, the more the deflection of the SWCNT is important.

We can conclude from Figs. 6(b) and 7 (b), that for the sensitivity $S(F)$ of the force sensor to be large, it is necessary to have a carbon nanotube that has a small chirality as possible and as long a nanotube length as possible.

A third series of calculations corresponded to a carbon nanotube of chirality $n = 9$ and fixed length of 200 nm and Young's modulus varying from $EX1 = 2.038\,1 \times 10^{12}$ Pa,

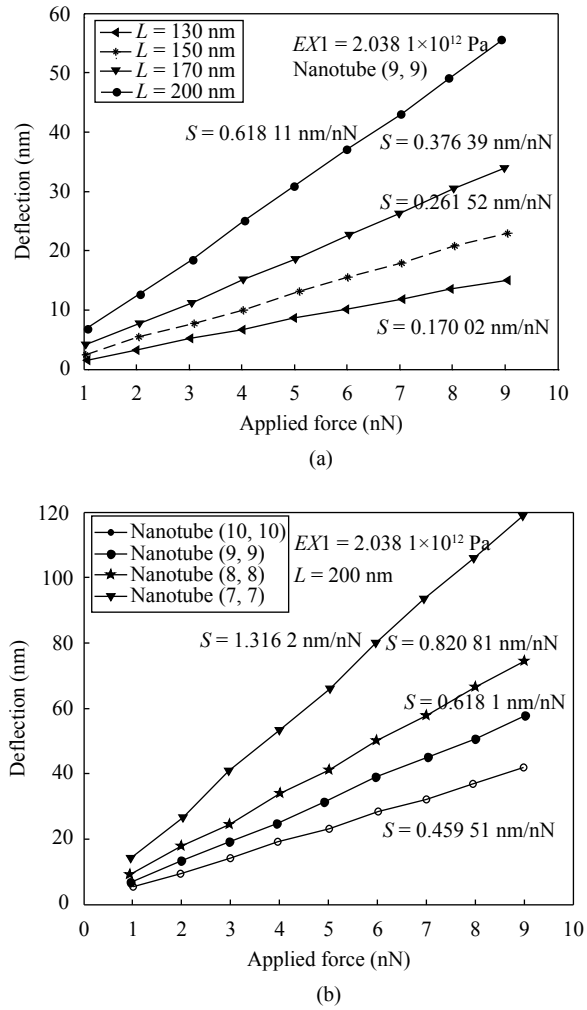

Fig. 6 Effect of nanotube length on (a) maximum deflection and (b) sensor sensitivity

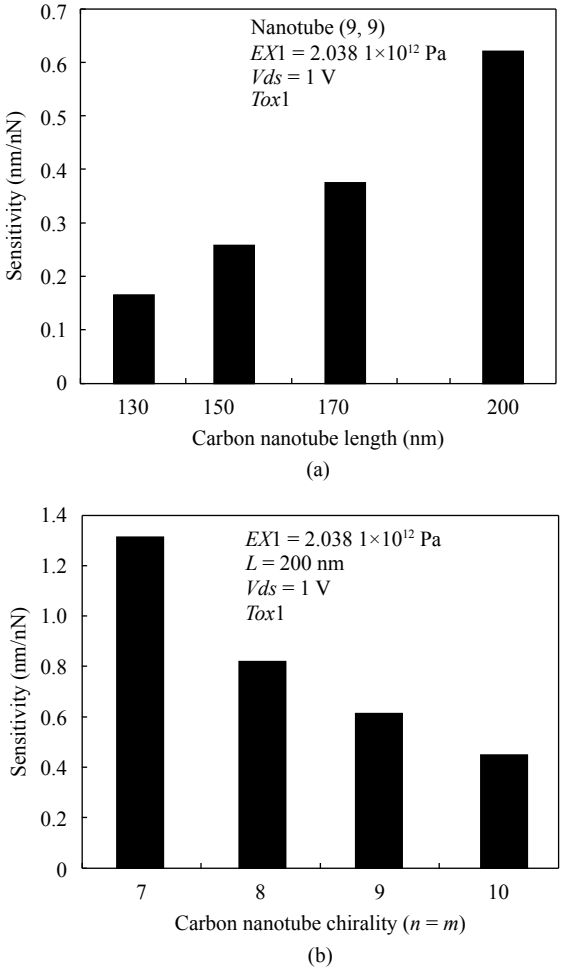

Fig. 7 Effect of the nanotube chirality on (a) maximum deflection and (b) sensor sensitivity

$EX2 = 2.305\,5\times10^{12}$ Pa, $EX3 = 2.430\,1\times10^{12}$ Pa, $EX4 = 2.449\,7\times10^{12}$ Pa, the results of simulations are shown in Fig. 8(a).

According to Fig. 8 (a), it is clear that when the Young's modulus is higher, the nanotube deflection decreases.

We calculated the sensitivity of the nano force sensor for a nanotube chirality $n = m = 9$ and length $L = 200$ nm for different values of Young's modulus. The results of the sensitivity are shown in Fig. 8 (b). Comparing Figs. 6 and 7 with Fig. 8, it is obvious that the effect of Young's modulus is much lower than that of both the nanotube length and diameter. We have found that the deflection of the carbon nanotube depends strongly on the geometric and physical parameters.

3 Electrical modeling of nano force sensor

The detection of the deflection of the studied nanotube in the preceding part can be detected by a capacitive measurement, for which purpose the carbon nanotube was used as a suspended gate of a the metal-oxide-semiconductor field-effect transistor (MOSFET). The variation in the applied force causes a variation in the capacitance of the gate-oxide transistor, the MOSFET itself may become a capacitive sensor. In the SG-MOSFET (suspended gate MOSFET) structure, the gate is suspended above the gate insulation (Fig. 9), the space between the suspended gate and the gate insulator is called a gap.

When a force is applied to the gate, it moves and the gate capacitance is changed, which causes the variation of the drain current and the threshold voltage. By detecting the threshold voltage electrically, the input force can therefore be measured. The structure in Fig. 9 is a schematic diagram of our capacitive nanoforce sensor.

Since the suspended gate field effect transistor is similar to a metal-oxide-semiconductor (MOS) transistor in its structure, the threshold voltage V_{Th} can be written in the case of a suspended gate transistor in the following form[22].

$$V_{Th} = W_G - W_{si} + 2\varphi_f - \frac{Q_{SS} - Q_{BO} \pm Q_{gap}}{C_T} \quad (10)$$

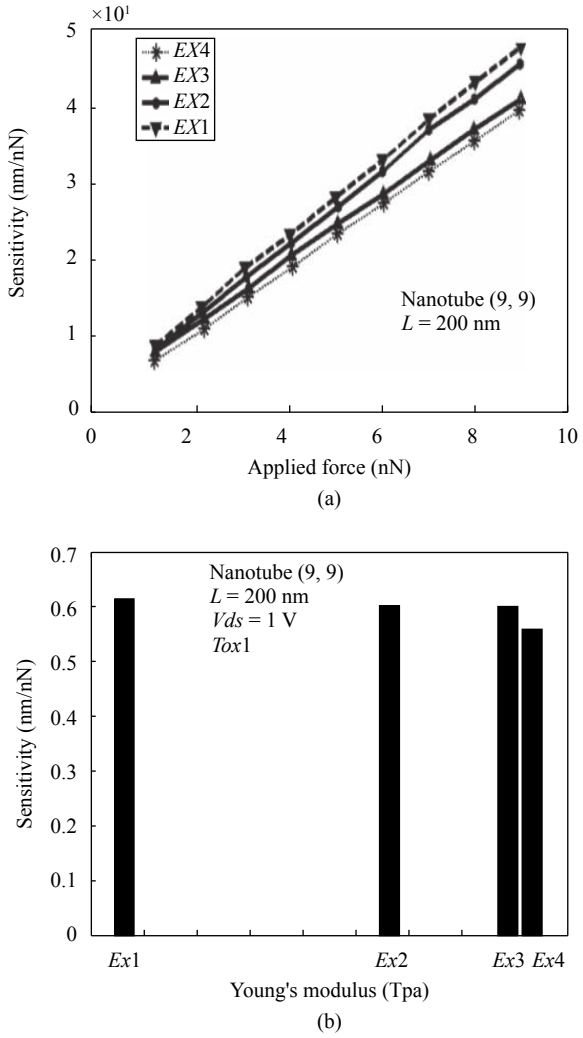

Fig. 8 Young modulus effect on (a) maximum deflection and (b) sensor sensitivity

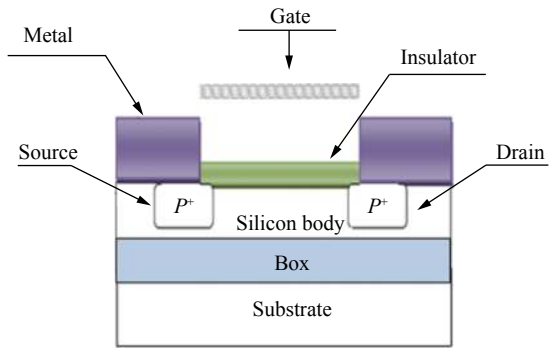

Fig. 9 Schematic diagram of our capacitive nanoforce sensor

$$\frac{1}{C_T}=\frac{1}{C_I}+\frac{1}{C_{gap}}=\frac{\varepsilon_0\varepsilon_{rox}}{Z_{gap}\varepsilon_{rox}+T_{ox}} \tag{11}$$

where W_G is the work function of the gate material, ϕ_f is the difference between the Fermi level and the intrinsic level, Q_{SS} is the charge in the gate insulator, C_I is the capacitance of the gate insulator, C_{gap} is the gap capacity, Q_{BO} is the space charge in the depletion region at the beginning of the strong inversion, Q_{gap} is the charge in the gap, ε_0 is the free space permittivity, ε_{rox} ($\varepsilon_{rox}=3.9$) is the relative dielectric permittivity of silicon dioxide, t_{ox} is the thickness of oxide layer and Z_{gap} is the air gap, the air gap relative permittivity equals to 1. When the suspended gate of the transistor is subjected to a force F, its position changes from Y_1 to Y_1-d, consequently the threshold voltage will change from V_{Th1} to V_{Th2}.

We used the TCAD-SILVACO (ATLAS) simulator to simulate the behavior of the suspended gate transistor of the nano force sensor, based on data from the previous section obtained by the finite elements method, where we performed a relation between the nanotube deflection and the applied force. By combining the results obtained by the finite elements method with that of SILVACO, the threshold voltage V_{Th} as a function of the applied force can be deduced. We describe the evolution of the threshold voltage characteristics as a function of the applied force F as well as the applied voltages Vds, Vgs, and the upper silicon oxide thickness ($Tox1=17$ nm, $Tox2=19$ nm $Tox3=22$ nm).

Fig. 10 illustrates the relationship between the threshold voltage of the transistor and the applied force.

From Fig. 10, we find that the increase of the applied force generates an increase in the threshold voltage value V_{Th}. Following the results shown in Figs. 10 (a)–10 (c), we can affirm that different geometrical parameters (upper oxide thickness of transistor, length and chirality of the carbon nanotube (CNT)) can affect the sensor response.

It can be seen that increasing the length of the nanotube causes an increase in the threshold voltage V_{Th}. On the other hand, increasing the nanotube diameter or increasing the thickness of the upper transistor oxide causes a reduction in the threshold voltage V_{Th}. It is evident from Figs. 10 (a)–10 (c) that the effect of the carbon nanotube diameter is much greater than that of the carbon nanotube length and the thickness of the transistor upper oxide.

It is noted according to Fig. 10 (b) that the variation in the threshold voltage V_{Th} observed seem to stabilize when the thickness of the air gap is zero ($Z_{gap}=0$). For an applied force $F>4$ nN, in the case of a nanotube with chirality $n=7$ and length 200 nm, the threshold voltage becomes constant $V_{Th}=-0.2$ V. However, this fact has no negative impact on the ability of the detection of the applied force because our target is to detect the weaker nanoscale. It can be seen from Fig. 10 (d) that it is obvious that when the nanotube has a lower young modulus, its threshold voltage is important. For the mathematical modeling of the nano force sensor response, we made a polynomial interpolation of the third degree. The third-order polynomial interpolation is very suitable for the mathematical modeling of the nano force sensor response based on a carbon nanotube, with a chirality 9 and of a

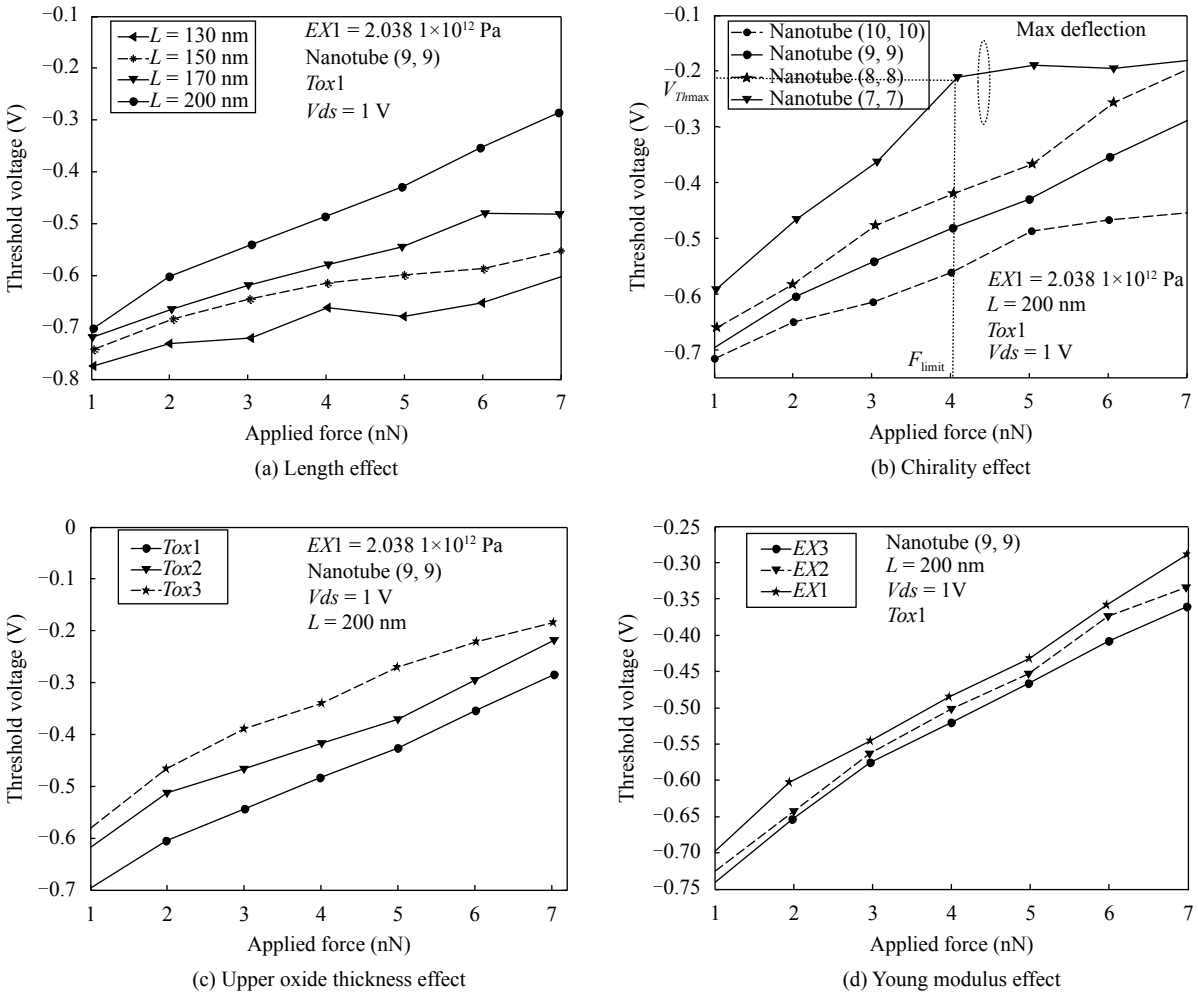

Fig. 10 Simulation of the threshold voltage as a function of the applied force under the physical and geometrical parameters effect

length 200 nm, the mathematical equation of this polynomial is given by (12) and presented in Fig. 11.

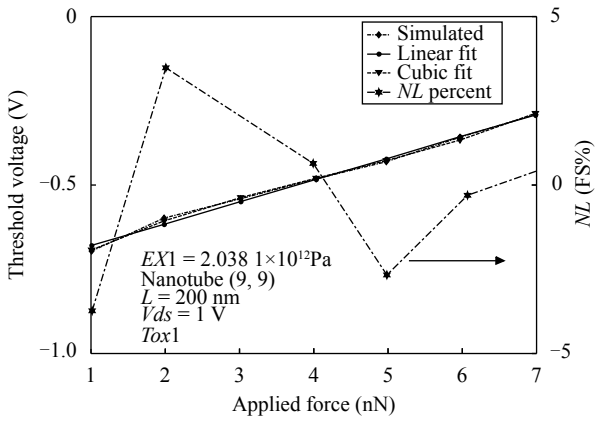

Fig. 11 Modeling of the threshold voltage as a function of the applied force

$$V_{Th} = (0.001\,503 \times F^3 + 0.018\,95 \times F^2 + 0.135\,3 \times F - 0.816\,9). \quad (12)$$

The non-linearity of the nano force sensor response is calculated by the following equation:

$$NL = 100 \times \frac{(V_{Th})_m - (V_{Th})_l}{FS} \quad (13)$$

where $(V_{Th})_m$ is the threshold measurement point, $(V_{Th})_l$ is the straights line of the least squares point for the same applied force and FS is the full scale response. The non-linearity value is expressed in 12 as a percentage of the full scale response (FS). The non-linearity response of the nanoforce sensor in function of applied force, for a nanotube (9,9) with a length of 200 nm, is shown in Fig. 11.

Fig. 12 (a) shows the effect of the nanotube length on the sensor sensitivity, it is found that the sensitivity of the sensor takes the values of 0.026 155 V/nN, 0.029 176 V/nN, 0.041 428 V/nN, 0.066 391 V/nN respectively when the length of the nanotube has the values 130 nm, 150 nm, 170 nm and 200 nm, respectively.

It is also observed from Fig. 12(b) that the sensitivity decreases from 0.124 31 V/nN to 0.066 391 V/nN to 0.046 445 V/nN when the nanotube chirality takes values $n=7$, $n=8$, $n=9$ and $n=10$ respectively. It is noted that,

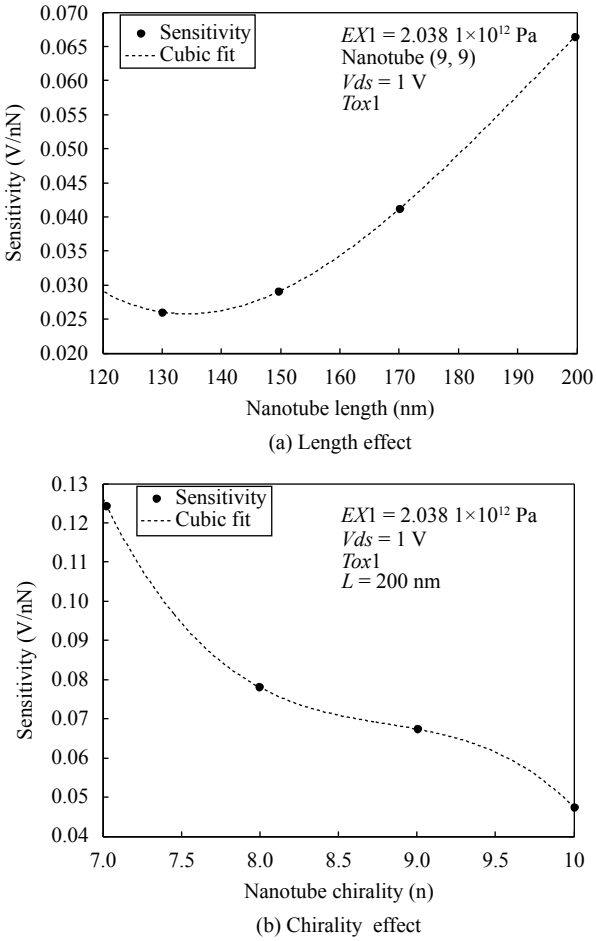

Fig. 12 Sensitivity characteristics

the sensitivity to the applied force is defined by (14).

$$S(F) = \frac{\Delta(V_{Th})}{\Delta F}. \tag{14}$$

After these results, we can conclude that to have a nano force sensor with high sensitivity, it is necessary to choose the longest nanotube with the shortest diameter possible.

It can be seen from Fig. 12 that the sensitivity obtained by our developed model can reach the value 0.12431 V/nN. On the other hand, the sensitivity obtained by previous studies, for example, the sensitivity of nano sensor developed by [23] is 0.011 V/nN. It is found that the sensitivity of our proposed nano force sensor is higher than the results of the literature.

4 Modeling of nano force sensor by neural networks

Artificial neural networks (ANNs) are used to model complex systems because of their highly multi-variable aspect and their strong non-linearity. In this study, we found that our nano force sensor exhibits a nonlinear characteristic, as well as the influence of different parameters on its response. For this purpose, neural networks have been adopted as a general approach of linearization in order to obtain a smart sensor. This involves associating an electronic structure for the corrections to the sensor. We have used the simulation results by the finite elements of the previous part as a database of the neural approach.

4.1 Artificial neural networks-direct model

The aim of this part is to develop a direct model based on artificial neural networks called "ANN-model", the latter is used to faithfully substitute the nano force sensor response of the model developed in the previous part. Artificial neural networks structures are organized around a set of cells (neurons) interconnected according to a certain architecture by weighted and modifiable links (bias/weights) during a procedure called training[24]. There are many applications of ANN in data analysis, model identification and control[25, 26].

Among different types of ANN, the multi-layer perceptron (MLP) is quite popular and used for current work. The MLP consists of three layers: an input layer, an output layer, and one or more hidden layers. Each layer consists of a predefined number of neurons. The neurons in the input layer act only as distributors of the input signals a_i to the neurons in the hidden layer. Each neuron j in the hidden layer summarizes its input signals a_i after weighing them by the connection weights w_{ij} according to the connections of the input layer and calculates its output value y_j of the neuron as function (sum f), while b is bias. The output value y_j is given by (15).

$$y_j = f\left(\sum_i^n w_{ij}a_i + b\right). \tag{15}$$

The output of the neurons in the output layer is calculated in a similar manner. The mean square error (MSE) between the predicted (estimated) and simulated (FEM) values of the output neurons MSE is defined by (16).

$$MSE = \frac{1}{2}\sum_j^N (y_{dj} - y_i)^2 \tag{16}$$

where y_{dj} is the desired value of the output neuron j and y_i is the FEM simulated output of this neuron, each weight w_{ij} is adjusted to reduce E as rapidly as possible. Fig. 13 illustrates the neural network developed for the estimation of the threshold voltage V_{Th}. The network produces a result (the threshold voltage V_{Th}) by propagating its initial inputs ([F, n, Tox, L, EX, Vds, Vgs]) through the various network neurons to the output.

The configuration of a neural network for the

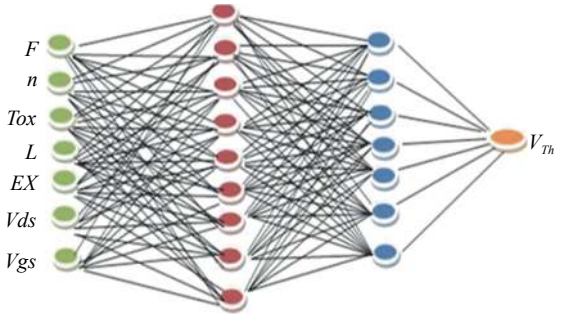

Fig. 13 Neural network layers diagram of the optimized architecture

threshold voltage estimation V_{Th} requires the choice of an adequate architecture, a training algorithm and activation functions.

In our case, the developed neural network is formed of four layers and the activation functions including the sigmoid function for the hidden layers and the function identity for the output layer. Our neural network has 7 inputs (F, n, Tox, L, EX, Vds, Vgs) and a single output (V_{Th}), all inputs are standardized to improve the performance of the network training process[26].

In our case, we have chosen MLP as the network type, the interest of this network is in its characteristic of universal approximation and its ease of implementation.

The optimization process of the previous network involves several steps: building the database, validating the structure of the neural network, correcting its weights and its training. The training and optimization of the network is accomplished by a program structured in Matlab.

Once the training is complete, it is necessary to test it on a database different from that used for training.

During the training and optimization of our network, different architectures are tested to determine the adequate number of layers and hidden neurons

Table 3 summarizes the network-optimized parameters for the sensor modeling.

The number of neurons in the first hidden layer is nine neurons, the second hidden layer has seven neurons and the model stabilizes after 1 200 iterations. From Fig. 14, it is easy to verify the reliability of our model for the prediction of the response of our nano force sensor over a wide applied force range from 1 nN to 7 nN.

The results obtained show a very good concordance explained by a high correlation coefficient for the training phase ($R_{tr}=0.998\,1$) the test phase ($R_{test}=0.997\,1$) and the validation phase ($R_{val}=0.996\,9$), this indicates that these results are very satisfactory.

4.1.1 Implementing of the direct neural model in PSPIC

The implementation of such a model in ORCAD-PSPICE was possible thanks to the improvements made on the latest versions of this software, which now allows a great flexibility in the description of the models. It is indeed possible to describe these with the aid of analog behavioral modeling "ABM" in which any type of equation linking the input variables to the output can be envisaged. These tools will allow us to easily implant our neural model of the nano force sensor in the PSPICE simulator.

Fig. 15 shows the neuronal model implanted as a component in the PSPICE simulator.

The "ABMs" blocks of the PSPICE simulator library and the results obtained during the design and optimization phase (optimal architecture, bias and network weight) are used to implement the model as a component in the library of the PSPICE simulator.

4.1.2 PSPICE simulation results

The validation of the model will consist in simulating our neural model in an electrical environment. The results of the simulation are presented in Figs. 16 (a) and 16 (b).

Table 3 Optimized parameters of the ANN-direct model

Database	Training base		821					
	Test base		410					
	Validation base		410					
Number of neurons	Input layer		7	Transfer function	1st hidden layer	Logsig		
	1st hidden layer		9		2nd hidden layer	Logsig		
	2nd hidden layer		7		Output layer	Linear		
	Output layer		1					
Input	F		n	L (nm)	Ex	Tox (nm)	Vgs	Vds
	Max	7 Nn	10	200	$2.430\,1\times10^{12}$	22	1.5 V	2 V
	Min	1 Nn	7	130	$2.038\,1\times10^{12}$	17	0.2 V	0.5 V
Output	V_{Th}		Test MSE			$7.315\,8\times10^{-5}$		
	Max	–0.182 2	Training MSE			10^{-5}		
	Min	–0.779 2						

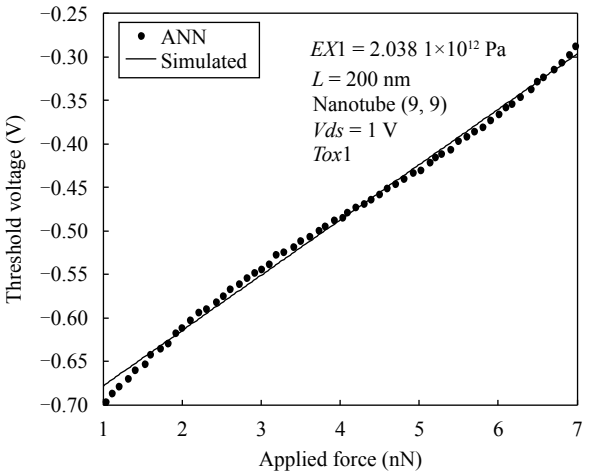

Fig. 14 Direct neuronal model performance

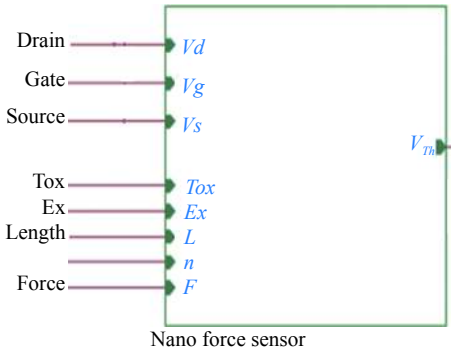

Fig. 15 Neuronal model implanted as a component in the PSPICE simulator

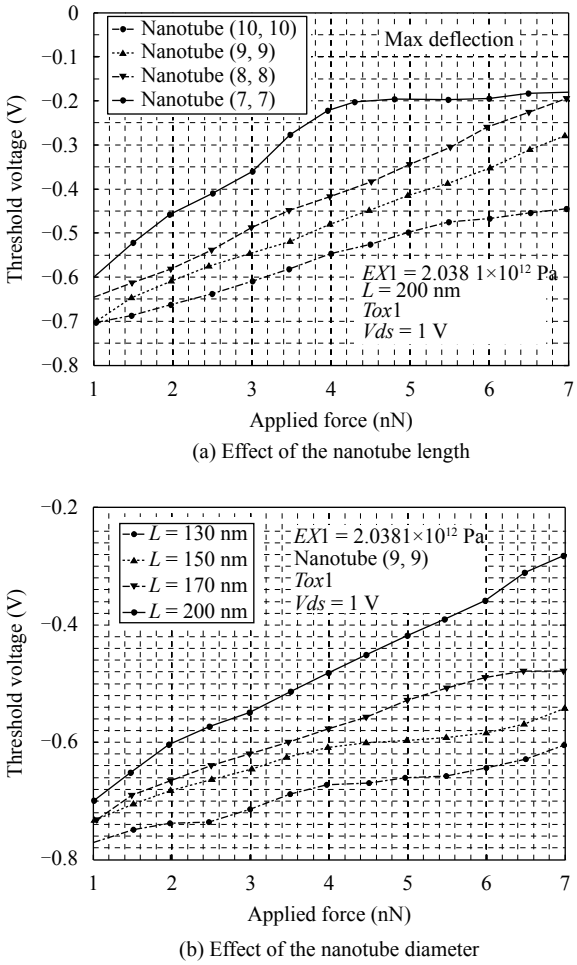

Fig. 16 PSPICE simulation results of the ANN direct model

According to these results, it is clear that the model designed and implemented in the PSPICE simulator accurately expresses the behavior of the nano force sensor in the electrical environment, taking into account the nonlinearity of the response. The simulation results show that the new nanoforce sensor model can be implemented as a component in the PSPICE library. The non-linearity of the sensor response poses a measurement problem, in this context the linearization of nano force sensor response is primordial to avoid measurement errors, which will be discussed in the next part.

4.2 Smart inverse ANN model (INV-ANN)

In order to have a linear response of our sensor, we need an inverse model INV-ANN, also called a smart model. For the development of this model, we begin by linearizing the response of the threshold voltage obtained using the neural networks, we choose a characterized database. The formation of the test and validation database is carried out by separating the training database and then we do the training of a neural network based on the back propagation algorithm. Finally the performance of the model obtained is verified with the test database. After the creation of the database, we proceed to carry out a simulation by neural networks, where we keep the same previous neural architecture. The number of hidden layers is two, the number of neurons used in each hidden layer is nine for the first layer and seven for the second layer, and the same choice of the activation functions type is also maintained. Fig. 17 shows the evolution of the MSE as a function of the number of iterations.

4.2.1 Performance measurement of the INV-ANN model using PSPICE

In order to test the performance of the smart model developed in an electrical environment, we have implanted it as an electrical component in the ORCAD-PSPICE simulator library.

Fig. 18 (a) shows the Direct-ANN model output curve with the INV-ANN model for a nanotube (9, 9) with a length 200 nm. In examining the results obtained in Figs. 18 (b) and 18 (c), we can say that they give excellent results. In effect, they deliver a linear output response.

Fig. 19 shows the difference between the desired correction model (inverse ANN model) and that obtained by

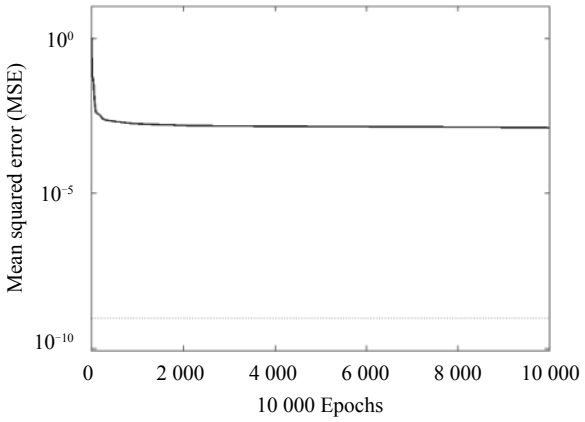

Fig. 17 Evolution of the MSE as a function of the number of iterations

the direct ANN model, this difference presents the linearization error for different values of the applied force.

5 Conclusions

In this paper, we proposed a new smart nano sensor specifically designed to detect and measure nano-newton-scale force using a structure consisting of a suspended carbon nanotube, this carbon nanotube is used as a suspended MOSFET gate. We have developed a three-dimensional model of the carbon nanotube based on the finite elements, the modeling has been done using the ANSYS simulator.

We have found through this study that the deflection of the carbon nanotube depends strongly on the geometric and physical parameters of the CNT. From the results obtained in this study, the increase in the applied force causes an increase in the value of the threshold voltage (V_{Th}) of the MOSFET. The sensitivity obtained by our model developed can reach up to 0.12431 V/nN, this sensitivity is superior to the results found in the literature.

Through this paper, we have shown that the artificial neural networks (ANNs) accurately express the behavior of the nano force sensor. The nano force ANN model, thus obtained, was implanted on the library of the PSPICE simulator as a component, which allowed us to simulate its operation on an electrical environment. We also proposed an INV-ANN model as a corrector component, for the nano force sensor. The purpose assigned to this component is the correction of the output signal of the sensor, in other words, to obtain a linear sensor. It should be noted that the difference between the two developed models is that: The first model is a behavioral modeling of the capacitive nano force sensor, whereas the second model plays the role of a correction component.

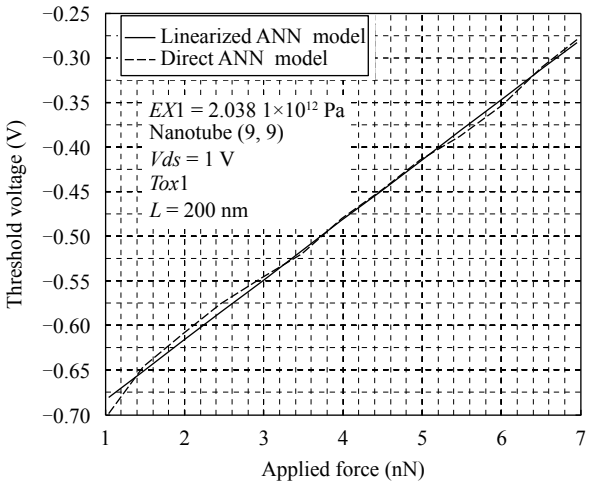

(a) PSPICE simulation results of the ANN direct and INV-ANN model

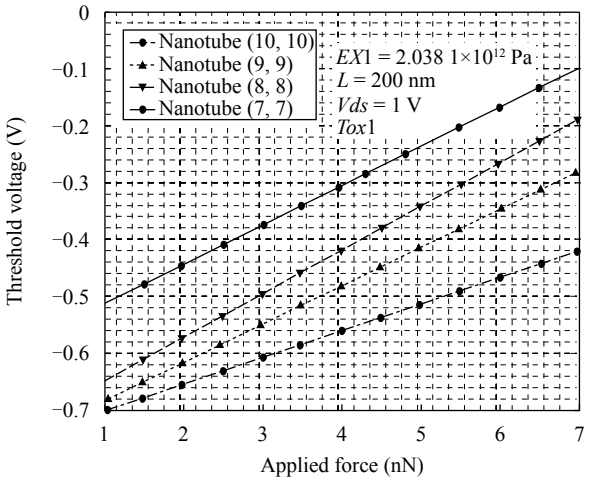

(b) Effect of the nanotube diameter

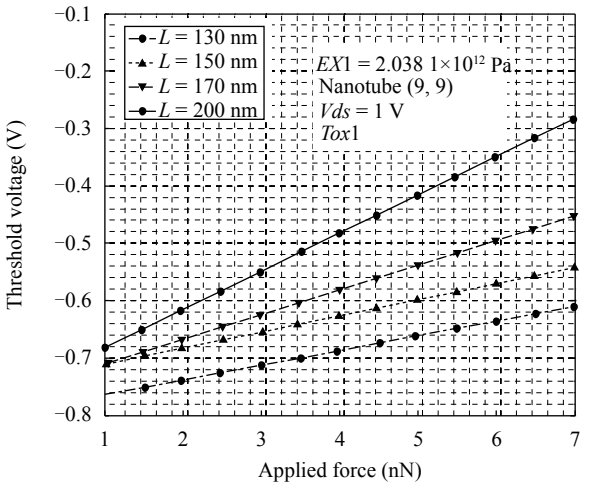

(c) Effect of the nanotube length

Fig. 18 Response of the corrector model

Acknowledgement

The authors would like to thank the Mechanical Engineering Laboratory of the University of Biskra, Algeria, for their important help and support in developing the numerical models using ANSYS simulator.

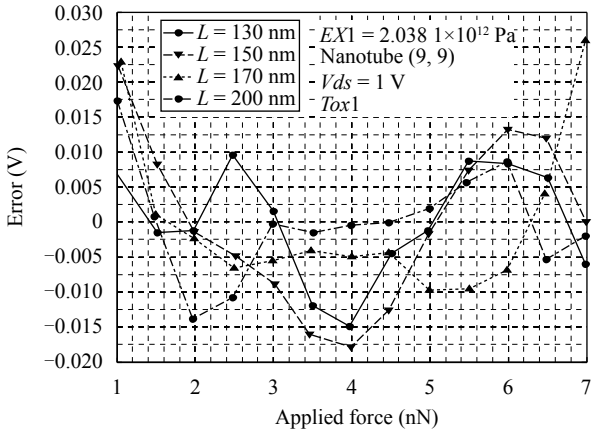

Fig. 19 Linearization error for different values of the applied force

References

[1] P. Rougeot, S. Régnier, N. Chaillet. Forces analysis for micro-manipulation. In *Proceedings of IEEE International Symposium on Computational Intelligence in Robotics and Automation*, Espoo, Finland, pp. 105–110, 2005. DOI: 10.1109/CIRA.2005.1554262.

[2] N. Kato, I. Suzuki, H. Kikuta, K. Iwata. Force-balancing microforce sensor with an optical-fiber interferometer. *Review of Scientific Instruments*, vol. 68, no. 6, pp. 2475–2478, 1997. DOI: 10.1063/1.1148171.

[3] M. Kalantari, J. Dargahi, J. Kövecses, M. G. Mardasi, S. Nouri. A new approach for modeling piezoresistive force sensors based on semiconductive polymer composites. *IEEE/ASME Transactions on Mechatronics*, vol. 17, no. 3, pp. 572–581, 2012. DOI: 10.1109/TMECH.2011.2108664.

[4] A. S. Krajewski, K. Magniez, R. J. N. Helmer, V. Schrank. Piezoelectric force response of novel 2D textile based PVDF sensors. *IEEE Sensors Journal*, vol. 13, no. 12, pp. 4743–4748, 2013. DOI: 10.1109/JSEN.2013.2274151.

[5] K. F. Lei, K. F. Lee, M. Y. Lee. A flexible PDMS capacitive tactile sensor with adjustable measurement range for plantar pressure measurement. *Microsystem Technologies*, vol. 20, no. 7, pp. 1351–1358, 2014. DOI: 10.1007/s00542-013-1918-5.

[6] E. Peiner, L. Doering. Force calibration of stylus instruments using silicon microcantilevers. *Sensors and Actuators A*, vol. 123–124, pp. 137–145, 2005. DOI: 10.1016/j.sna.2005.02.031.

[7] R. Pérez, N. Chaillet, K. Domanski, P. Janus, P. Grabiec. Fabrication, modeling and integration of a silicon technology force sensor in a piezoelectric micro-manipulator. *Sensors and Actuators A*, vol. 128, no. 2, pp. 367–375, 2006. DOI: 10.1016/j.sna.2006.01.042.

[8] T. L. Li, L. Q. Li, G. Y. Zhang. A nano-scaled force sensor based on a photonic crystal nanocavity resonator and a microcantilever. *ECS Journal of Solid State Science and Technology*, vol. 3, no. 7, pp. Q146–Q151, 2014. DOI: 10.1149/2.0151407jss.

[9] L. Q. Li, T. L. Li, F. T. Ji, W. P. Song, G. Y. Zhang, Y. Li. The effects of optical and material properties on designing of a photonic crystal mechanical sensor. *Microsystem Technologies*, vol. 23, no. 8, pp. 3271–3280, 2017. DOI: 10.1007/s00542-016-3186-7.

[10] S. Iijima. Helical microtubules of graphitic carbon. *Nature*, vol. 354, no. 6348, pp. 56–58, 1991. DOI: 10.1038/354056a0.

[11] A. Eatemadi, H. Daraee, H. Karimkhanloo, M. Kouhi, N. Zarghami, A. Akbarzadeh, M. Abasi, Y. Hanifehpour, S. W. Joo. Carbon nanotubes: Properties, synthesis, purification, and medical applications. *Nanoscale Research Letters*, vol. 9, no. 1, Article number 393, 2014. DOI: 10.1186/1556-276X-9-393.

[12] O. Kanoun, C. Müller, A. Benchirouf, A. Sanli, T. N. Dinh, A. Al-Hamry, L. Bu, C. Gerlach, A. Bouhamed. Flexible carbon nanotube films for high performance strain sensors. *Sensor*, vol. 14, no. 6, pp. 10042–10071, 2014. DOI: 10.3390/s140610042.

[13] Y. G. Li, R. Ahuja, J. A. Larsson. Communication: Origin of the difference between carbon nanotube armchair and zigzag ends. *The Journal of Chemical Physics*, vol. 140, no. 9, Article number 091102, 2014. DOI: 10.1063/1.4867744.

[14] L. Marty, A. Iaia, M. Faucher, V. Bouchiat, C. Naud, M. Chaumont, T. Fournier, A. M. Bonnot. Self-assembled single wall carbon nanotube field effect transistors and AFM tips prepared by hot filament assisted CVD. *Thin Solid Films*, vol. 501, no. 1–2, pp. 299–302, 2006. DOI: 10.1016/j.tsf.2005.07.218.

[15] C. H. Ke, H. D. Espinosa. Feedback controlled nanocantilever device. *Applied Physics Letter*, vol. 85, no. 4, pp. 681–683, 2004. DOI: 10.1063/1.1767606.

[16] D. Mtsuko, A. Koshio, M. Yudasaka, S. Iijima, M. Ahlskog. Measurements of the transport gap in semiconducting multiwalled carbon nanotubes with varying diameter and length. *Physical Review B*, vol. 91, no. 19, Article number 195426, 2015. DOI: 10.1103/PhysRevB.91.195426.

[17] X. L. Tang, A. El Hami, K. El-Hami. Mechanical properties investigation of single-walled carbon nanotube using finite element method. *Key Engineering Materials*, vol. 550, pp. 179–187, 2013. DOI: 10.4028/www.scientific.net/KEM.550.179.

[18] C. Mungra, J. F. Webb. Free vibration analysis of single - walled carbon nanotubes based on the continuum finite element method. *Global Journal of Technology & Optimization*, vol. 6, no. 2, Article number 1000173, 2015. DOI: 10.4172/2229-8711.1000173.

[19] C. Y. Li, T. W. Chou. A structural mechanics approach for the analysis of carbon nanotubes. *International Journal of Solids and Structures*, vol. 40, no. 10, pp. 2487–2499, 2003. DOI: 10.1016/S0020-7683(03)00056-8.

[20] D. H. Wu, W. T. Chien, C. S. Chen, H. H. Chen. Resonant frequency analysis of fixed-free single-walled carbon nanotube-based mass sensor. *Sensors and Actuators A*, vol. 126, no. 1, pp. 117–121, 2006. DOI: 10.1016/j.sna.2005.10.005.

[21] S. Prabhu, S. Bhaumik, B. K. Vinayagam. Finite element modeling and analysis of zigzag and armchair type single wall carbon nanotube. *Journal of Mechanical Engineering Research*, vol. 4, no. 8, pp. 260–266, 2012. DOI: 10.5897/JMER12.025.

[22] I. H. Song, P. K. Ajmera. A laterally movable gate field effect transistor. *Journal of Microelectromechanical Systems*, vol. 18, no. 1, pp. 208–216, 2009. DOI: 10.1109/JMEMS.2008.2008623.

[23] F. Djeffal, Z. Dibi, M. L. Hafiane, D. Arar. Design and simulation of a nanoelectronic DG MOSFET current source using artificial neural networks. *Materials Sciences and Engineering: C*, vol. 27, no. 5–8, pp. 1111–1116, 2007. DOI: 10.1016/j.msec.2006.09.005.

[24] F. Djeffal, S. Guessasma, A. Benhaya, M. Chahdi. An analytical approach based on neural computation to estimate the lifetime of deep submicron MOSFETs. *Semiconductor*

Science and Technology, vol. 20, no. 2, pp. 158–164, 2005. DOI: 10.1088/0268-1242/20/2/010.

[25] F. Menacer, A. Kadri, F. Djeffal, Z. Dibi, H. Ferhati. Modeling of boron nitride-based nanotube biological sensor using neural networks. *Proceedings of the 17th International Conference on Sciences and Techniques of Automatic Control and Computer Engineering*, Sousse, Tunisia, 2016. DOI: 10.1109/STA.2016.7951987.

[26] F. Menacer, A. Kadri, F. Djeffal, Z. Dibi. Modeling and investigation of smart capacitive pressure sensor using artificial neural networks. *Proceedings of the 6th International Conference on Systems and Control*, Batna, Algeria, 2017. DOI: 10.1109/ICoSC.2017.7958746.

Farid Menacer received the B. Eng. degree in electronics control, and the M. Eng. degree in instrumentation from Batna University, Algeria in 1996 and 2011, respectively.

His research interests include neuronal networks, sensors and intelligent system.

E-mail: menacer_farid@yahoo.fr (Corresponding author)

ORCID iD: 0000-0001-5067-9996

Abdelmalek Kadr received the B. Eng. degree in electronics control, and the M. Eng. degrees in instrumentation from Batna University, Algeria in 1995 and 2012, respectively.

His research interests include neuronal networks, sensors, intelligent system and nanotechnology

E-mail: kadmalekamis@yahoo.fr

Zohir Dibi received the B. Sc. degree in electronics engineering from University of Setif, Algeria in 1994, the M. Eng. and Ph. D. degrees from University of Constantine, Algeria in 1998 and 2002, respectively. He has been the head of Electronics Department. He is currently an assistant professor in Department of Electrical and Electronic Engineering and vice-dean of the Faculty of Engineering, Batna University, Algeria.

His research interests include neural networks, sensors, smart sensors, and organic devices.

E-mail: zohir_dibi@yahoo.fr